Journal of Electronic Imaging 15(2), 1 (Apr–Jun 2006)

Structure and characterization of an enhanced laser-scanning endoscope based on microelectromechanical mirrors

Hansjörg Albrecht
Laser-und Medizin-Technologie GmbH
Fabeckstr. 60-62
D-14195 Berlin, Germany

Panagiotis G. Papageorgas
Dimitris Maroulis
Nikiforos Theofanous
Stavros Karkanis
University of Athens
Department of Informatics and Telecommunicaitons
Panepistimiopolis, Ilissia
15784 Athens, Greece

Bernd Wagner
Fraunhofer Institute for Silicon Technology
Fraunhoferstraße 1
25524 Itzehoe, Germany

Marc Schurr
University of Tubingen
Waldhornlestraße 22
72072 Tubingen, Germany

Christian Depeursinge
Swiss Federal Institute of Technology (EPFL)
Institute of Applied Optics
CH-Ecublens, CH-1015 Lausanne, Switzerland

Arianna Menciassi
Scuola Superiore Sant' Anna
ARTS & MiTech Lab. via Carducci 40
56127 Pisa, Italy

Abstract. *A miniaturized laser-scanning endoscope is presented that makes use of a composite laser beam for color imaging. A novel approach is followed in the device, which is based on scanning the target tissue with the laser beam using two miniaturized MEMS (microelectromechanical systems) micromirrors and employs specific collection, detection, and postprocessing of the scattered light for reconstructing a color image of the tissue. A resolution of the order of* 16 line pairs/mm *is achieved for a working distance of* 50 mm *while the focal depth is larger than* 5 mm. *Key considerations of the system design are presented, along with results on the operation of the micromirrors, an analysis of the optical design of the endoscope head, and remarks on the assessment of image quality. © 2006 SPIE and IS&T.* [DOI: 10.1117/1.2194890]

Paper 05055R received Apr. 6, 2005; revised manuscript received Oct. 19, 2005; accepted for publication Dec. 15, 2005. This paper is a revision of a paper presented at the SPIE conference on Novel Optical Instrumentation for Biomedical Applications, June 2003, Munich, Germany. The paper presented there appears (unrefereed) in SPIE Proceedings Vol. 5143.
1017-9909/2006/15(2)/1/0/$22.00 © 2006 SPIE and IS&T.

1 Introduction

Most of the medical endoscopes today employ CCD or CMOS sensors for video imaging.[1,2] For illumination of the target tissue, optical fiber bundles transfer the light from external sources to the head of the endoscope. Fiber bundles are also used for the detection of the backscattered light, but in advanced endoscopes the imaging sensor is directly embedded into the endoscope head with its resolution to be one of the limiting factors of the endoscope performance.

To overcome the resolution limitations of embedded im-

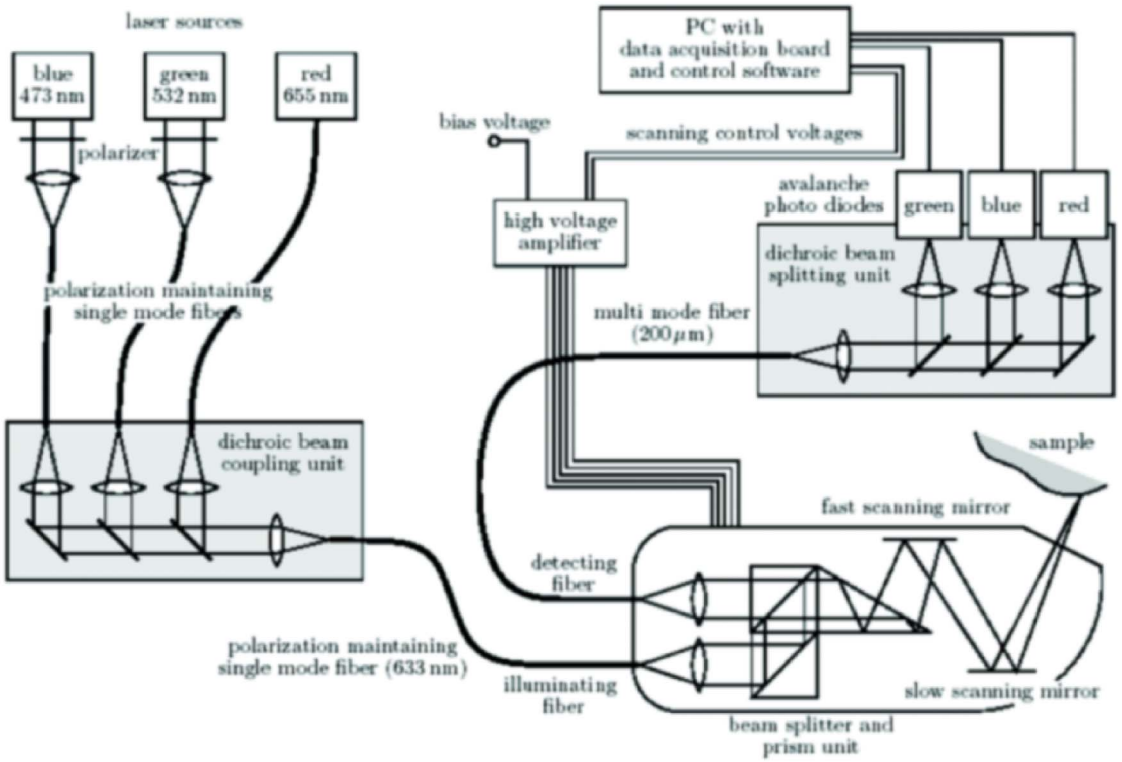

Fig. 1 Three-color laser scanning endoscopy system. The three laser wavelengths are provided through a polarization-maintaining fiber to the endoscope for illumination. The backscattered light is led by a multimode fiber to the detection unit.

age sensors, a novel alternative technology based on laser scanning has been conceived and implemented, and is presented in this paper. One important feature of this technology is that the imaging is performed using a composite laser beam that scans the target tissue for illumination, and the backscattered optical signal is detected and used for the reconstruction of the tissue image. The small dimension of the laser spot used for illumination provides the high resolution required. This technology known as "flying spot imaging"[3] has been proposed in imaging systems for biomedical applications such as in laser scanning microscopy[4,5] (LSM), confocal laser scanning microscopy[6] (CLSM), and optical coherence tomography[7] (OCT). In addition, microelectromechanical systems (MEMS) micromirrors have been proposed[5,8] for CLSM endoscopic imaging, providing small fields of view (of the order of 1 mm^2) and resolutions of the order of 500 lines/mm, while they normally utilize one wavelength for illumination and detection. What differentiates the endoscope under presentation with the just referenced laser scanning systems is that it combines color imaging with a large field of view (of the order of 20×20 mm), high resolution, and a focal depth of the order of 5 mm by employing appropriate MEMS micromirrors and optical design.

In this paper, the key considerations for the system design are first presented with emphasis on the optical design of the endoscope head, followed by a short description of the laser-scanning micromirrors developed, a presentation of the data acquisition and control unit, and the optical characterization methods applied for the objective evaluation of imaging performance. Finally, imaging results for artificial and biological objects are given together with a discussion of the overall endoscope performance.

2 System Components and Operation

This section describes the more important components of the laser-scanning endoscope under presentation, which is depicted in Fig. 1, and their functional relations. The endoscope system comprises a three-color laser illumination unit, an endoscope head with embedded scanning micromirrors and microoptics, a three-color detection unit, and a data-acquisition processing and control unit. In the optical part of the endoscope head, the laser light beam is directed by means of the two micromirrors upon the target tissue, and the corresponding reflected and backscattered light is collected by the photodetection system (employing one avalanche photodiode for each color) via an assembly of lens and prisms.

The goal for RGB color imaging would be to reproduce the same colors as they are perceived with our eyes. Our eyes are sensitive in the 400- to 700-nm range with a maximum sensitivity of the individual sensors at 450, 540, and 570 nm. On the other hand, each sensor has a broad sensitivity with a half width of approximately 80 nm, and in normal surroundings, objects are illuminated with "white light," resulting in a broad spectrum. In the case of laser illumination, three very narrow spectral light distributions are used for illumination and detection. It is impossible to have the same color measurement as we have with our eyes for all objects. It is only possible to have for a certain class of objects a similar color measurement by adjusting the

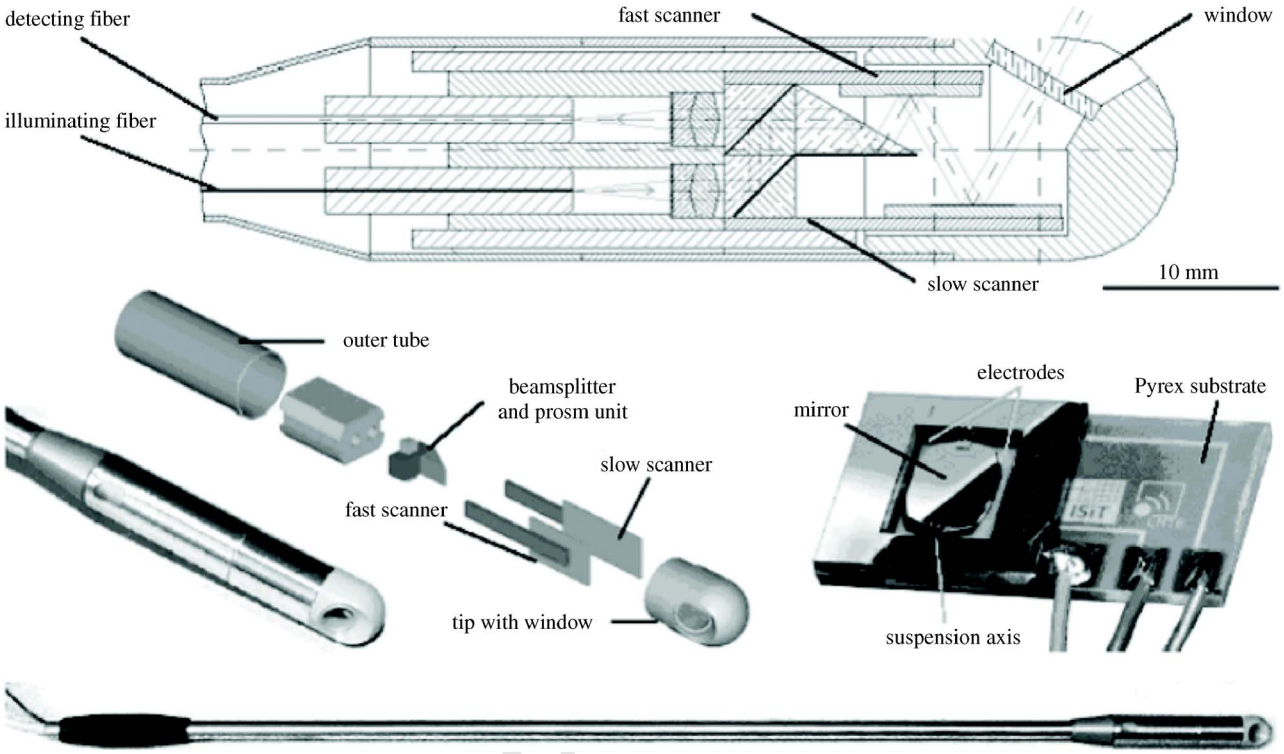

Fig. 2 Top, optomechanics of the scanning endoscope head; center from left to right, photograph of the assembled head, schematic of the subcomponents of the head, and photograph of the micromachined mirror for the fast scanning axis; bottom, complete endoscope head.

relative sensitivity of the three colors by an appropriate choice of the wavelengths for the illumination lasers. The wavelength selection was done according to the tissue spectral behavior and for the specific medical applications planned.

The scanning imaging operation performed is similar to the z-scanning operation of a CRT screen. Instead of an electron-beam we used two scanning micromirrors and a composite laser beam by combining three color laser beams. The two scanning micromirrors move around their axes, which are perpendicular each to another. One scanning micromirror moves slowly compared to the other in a quasi-static operation, deflecting the laser beam on the target tissue vertically, and can be compared to the line change operation of a CRT screen. Each rotation of the slow mirror corresponds to a single frame of the scanned area. The other mirror moves fast and in resonant mode, deflecting the laser beam on the target tissue horizontally and can be compared to the line scanning operation of a CRT screen. The combined motion of these mirrors results in the laser scanning operation of the target area. The optoelectronic processing of the backscattered optical signal with the corresponding subsystems results in the image reconstruction of the scanned area.

2.1 *Optical Design Considerations for the Endoscope Head*

The endoscope head is the main part of the entire system. Its optical components are fibers for illumination and detection with collimating microlenses, a unit consisting of two polarizing beamsplitters, a prism for beam deflection, and the micromachined scanning mirrors. To reject the specular component from our reflectance images we used the cross-polarization imaging technique by separating the illumination and the detection paths using polarized laser sources and the appropriate beamsplitters. In the optical arrangement followed, the mirrors are in a fixed position in relation to the beamsplitters and the prism, as shown in Figs. 1 and 2. This specific design provides the appropriate mechanism for micromirrors replacement, together with shock resistance, easy assembly, and a simple adjustment procedure. Furthermore, with this construction we faced a serious supplier problem, as it was not possible to manufacture the beamsplitter cube of 3×3 mm as originally designed. Two beamsplitters with dimensions of 4×4 mm were used together, leading to an enlargement of the endoscope head diameter to 12.5 mm in total.

The specifications that the presented endoscope should meet were a working distance of 50 mm, a focal depth greater than 5 mm, and a resolution of the order of 50 μm [or 20 line pairs/mm (lp/mm)] with an overall diameter for the endoscope head of the order of 12 mm. The critical design parameters of the endoscope system that must be considered to meet these specifications are not completely independent, so appropriate compromises were necessary. Starting from the working distance of 50 mm and the required resolution and focal depth, the numerical aperture (NA) of the imaging lens was first determined.

2.1.1 *Resolution Considerations*

In flying spot imaging as is used in the endoscope under description, the laser illumination is focused on the object

and the scattered light then emerges from a larger spot that is imaged onto the detection fiber. With the laser-scanning illumination, the object is already resolved as the emerging photons arrive with a higher probability from the small area illuminated by the laser spot. In detection, by imaging of a small spot of the backscattered light, the resolution and contrast can be improved, but with a strong loss of light intensity and a strong reduction of focal depth. Thus, for our requirements, a large spot imaging was preferred. This procedure is just the inverse of that followed in standard imaging. By minimizing the illumination spot size, the resolution can be improved and is determined mainly from the optics used for illumination, since in the proposed design the detection and illumination paths are separated.

The resolution of an imaging system is measured with its point spread function (PSF), which results from the convolution of the PSFs of the image sensor and the optics used. As a result, the PSF of the imaging system will be broader than either the objective lens PSF or that of the image sensor. To a reasonable approximation, the width of the imaging system PSF will be[4] the square root of the sums of the squares of the widths of the lens and sensor PSFs.

For a diffraction-limited lens with a focal distance f_{obj}, a diameter D, and numerical aperture NA, the Rayleigh criterion of resolution states that two point sources can be distinguished if they are separated by at least a distance (referenced in the object or focal plane) that is equal to

$$\Delta d = 1.22\frac{\lambda f_{\mathrm{obj}}}{D} = 0.61\frac{\lambda}{\mathrm{NA}}. \quad (1)$$

From Eq. (1) and under the assumption that the image sensor resolution contribution is small, it results that for high resolution (small Δd), the NA of the lens used for light collection from the target area must be high. On the other hand, another important optical design parameter is the focal depth. The focal depth can be calculated in different ways. One can set as a criterion an increase of the spot diameter by a factor of 2, which gives the value of two times the Rayleigh length (Gaussian optics):

$$\Delta z = 2\frac{\pi\Delta d^2}{\lambda} = 2\frac{0.61^2\pi\lambda}{\mathrm{NA}} \approx \frac{2\lambda}{\mathrm{NA}}. \quad (2)$$

But this definition does not take into account the fact that for a large NA, the spot diameter is much smaller than the useful resolution in medical application, and the defocused spot diameter as well. A criterion that fits the requirements better in a medical application is the setting of an absolute value of the desired spot diameter (d_{acc}) acceptable for imaging:

$$\Delta z = \frac{2\lambda}{\pi\mathrm{NA}}\left[\left(\frac{d_{\mathrm{acc}}\pi\mathrm{NA}}{2\lambda}\right)^2 - 1\right]^{1/2}. \quad (3)$$

Setting the upper limit of the spot size to 50 μm and a lower limit of the focal depth to 5 mm (for an acceptable spot diameter of 0.1 mm) from Eqs. (1) and (3) we calculated a useful overlapping range of 0.006 to 0.02 for the NA (Ref. 9). An NA of 0.015 was finally selected. Emerging from a monomode fiber, the laser beam is focused to the image plane where the laser spot radius is approximately 50 μm, while for the imaging system of Eq. (1) for an NA of 0.015 gives Δd=21.6 μm. Accordingly, the resulting PSF can be approximated with the square root of the sum of squares of the laser spot radius and the calculated Δd, resulting in a resolution of 53 μm, which is close to the targeted specification for resolution of 20 lp/mm.

In imaging systems, the aperture size, the shutter speed, and the illumination determine important image quantities such as the depth of focus and the motion blur that will be present. In CCD- or CMOS-based imaging systems, if the illumination is high, the aperture size can be small and the shutter speed high so the motion blur can be controlled to correspond to less than a pixel, and the imaged object seems to be still while the depth of focus is small. Slowing the shutter speed to compensate for low light conditions can result in a blurred image. In the described scanning system, the depth of focus is large, the aperture is high, and the shutter does not exist. The shutter speed parameter can be approximated in a scanning system with the acquisition time of each pixel, which is very small (of the order of microseconds) so the motion blur can be avoided. Of course, if the object moves, the resulting picture will not be correct (even without motion blur), and the imaging speed must be increased accordingly and within the limits of the oscillating frequency of the fast mirror and the bandwidth limitations of the photodetector and data acquisition boards used.

2.1.2 *Optical signal detection*

The endoscope was properly designed for the detection of the light backscattered from the object (tissue) rather than the light returning by Fresnel reflection from the sample surface. This feature was an important design consideration, as the endothelium is naturally covered by a liquid film, the reflection on which does not convey any information concerning the tissue structure. Another advantage resulting from this design, as compared with CCD-based endoscopes, is that scattered light carries information about layers below the tissue surface. Thus, the laser-scanning endoscope becomes a multiwavelength measurement tool specific for elastic light scattering. The rejection of Fresnel reflection is achieved by using a linearly polarized illumination and extinction in the detection path of the light with this polarization, by means of an appropriate analyzer. This is realized with a polarization-dependent beamsplitter in front of the collimating lens and before the detection fiber.

Due to the proceding considerations, polarized illumination was chosen. The first source, which was a red diode laser source (655 nm), provides a directly polarized output, while the frequency-doubled diode-pumped solid state lasers for the green (532-nm) and blue (457-nm) wavelengths must be beam-shaped and externally polarized before their coupling into the optical fiber.

In the diffusion regime, i.e., when scattering dominates absorption, the backscattering can be easily estimated. In that case, the total amount of backscattered light is given by[10]

Table 1 Transmission losses in the illumination and detection paths.

Illumination Path from Laser to Sample				Detection Path from Sample to Photodetector			
Wavelength (nm)	650	532	457	Wavelength (nm)	650	532	457
Polarization, beam shaping	1	0.5	0.34	Polarization	0.5	0.5	0.5
Fiber coupling	0.9	0.15	0.44	Endoscopic head	0.36	0.25	0.16
Beam coupling unit	0.9	0.7	0.7	Detecting fiber coupling	0.7	0.7	0.7
Illumination fiber coupling	0.5	0.2	0.2	Beamsplitter unit	0.9	0.8	0.7
Endoscopic head	0.3	0.2	0.1	Gain of avalanche diode	0.7	0.4	0.3
Depolarisation	1	0.9	0.67				
Total transmission loss in the illumination path	0.12	0.0019	0.0014	Total transmission loss in the detection path, τ_{det}	0.066	0.022	0.007
Laser power (mW)	10	100	100	R^{Ω} (10^{-4})	0.81	0.56	0.67
Power on tissue (mW)	1.2	0.19	0.14	$\tau_{det}\,R^{\Omega}$ (10^{-6}); total transmission loss in the detection path for the angle Ω	5.4	1.02	0.49

$$R_{\text{total}} = \frac{\alpha}{2\pi}\left(1 + \exp\left\{-\frac{4}{3}A\sqrt{[3(1-\alpha)]^{1/2}}\right\}\right) \times \exp\{-\sqrt{[3(1-\alpha)]^{1/2}}\}, \quad (4)$$

where α is the optical albedo of the target, and A is a parameter describing the internal reflection, which depends on the refractive index. Due to the chromatic dependence of relevant coefficients, the amount of the backscattered light around the illuminating spot is not the same for all wavelengths. Obviously, the imaging sensitivity for each channel will depend on the radius of the region from which light is collected. If the detection region is small, only a reduced amount of the total backscattered light is detected. As the resolution of the image depends mainly on the size of the illumination spot, a large detection region on the object plane can be chosen to increase sensitivity. In the realized endoscopic head a detecting fiber with a 200-μm core diameter was used, leading to a detection region with a 2 -mm diameter in the object plane.

In endoscopy, the imaged object must be at a distance l_{obj} of up to 50 mm from the imaging optics. At the same time, the size of the mirrors limits the beam diameter D and therefore the corresponding NA is small. In our endoscopic head, a NA=0.015 was realized and with an object distance of l_{obj}=50 mm, the amount of light backscattered within a small angle Ω was found to be in the order of $R^{\Omega}=0.5\times10^{-4}$. This result was ascertained by Monte Carlo simulation. In addition to the loss of light caused by absorption and backscattering through the imaged object, there are significant losses on the illumination path from the laser to the object and then back to the detector. Table 1 gives the loss factors (ratio of output versus input optical power) in the illumination and the detection paths to estimate the signal levels of the photodetectors used and for each specific illumination wavelength. The wavelength-dependent reflectivity of the two scanning mirrors have a major contribution, since losses at the mirror surfaces occur in both the illumination and the photodetection path and are given as endoscope head losses in Table 1. The main problem, which could not be solved in this specific realization, is the low signal mainly for the green and blue channels. Besides the low efficiencies of fiber coupling, the very low reflectance of the two scanning mirrors is the major reason for that. A high mirror reflectance is very important, because the illumination laser power is reduced two times and the backscattered light is reduced again two times by the mirrors. The low reflectance of 0.6 for the red, 0.5 for the green, and 0.4 for the blue channel (which results in loss factors of 0.36, 0.25, and 0.16 in the endoscope head, as given in Table 1) reduces the theoretical signal by factors of about 8 for the red, 16 for the green, and 40 for the blue channel. From Table 1 it results that the power levels of the optical signals that must detected from the three photodetectors are 6.48, 0.19, and 0.068 nW for the red, green, and blue channels, respectively (power on tissue multiplied by the $\tau_{\text{det}}R^{\Omega}$ in the last row of Table 1 and for each wavelength).

Two photodetectors were used in the realization of the endoscope. The C5460 avalanche photodiode (APD) from Hamamatsu has an active area with a diameter of 1.5 mm, a frequency bandwidth (−3 dB) from dc to 10 MHz, and a sensitivity of 0.8 nW for a signal-to-noise level of 1. This photodetector, according to the Table 1 calculations should have the necessary sensitivity only for the red channel while the supported bandwidth is high enough for video rates. An alternative realization for low signal levels was based on the C5460-1 APD, which is similar to the C5460 a bandwidth of 100 kHz and a sensitivity of 0.005 nW for a signal-to-noise level of 1. This low-bandwidth realization was finally used for color imaging since the achieved optical power levels for the blue and green levels were not adequate for the C5460 photodetector originally planned. The dynamic ranges of the detected optical signal for the

C-5460-1 APD according to the optical power calculations of Table 1 were estimated to be 62 dB for the red channel, 16 dB for the green channel, and 11 dB for the blue channel, approximately.

2.1.3 *Image frame rate and sampling frequency considerations*

The overall endoscope bandwidth results from the combination (multiplication in the frequency domain) of the endoscope head, the optical detector, and the acquisition board bandwidths. The maximum frequency of oscillation of the fast mirrors realized determines the line scan rate and the endoscope head bandwidth. In addition, the field-of-view (FOV) requirements in combination with the maximum optical resolution that must be resolved determines the minimum number of samples that must be acquired, which when combined with the line scan rate gives the minimum pixel sampling frequency.

For the specific realization and starting from the maximum frequency of the fast mirrors realized of 1.2 kHz, the line-scanning line frequency for bidirectional scanning (the scanning performed in both directions of the laser beam) is calculated to be 2.4 kHz, resulting in a line scan time of 416 μs.

According to the Nyquist sampling theorem and to resolve the designed optical resolution of 50 μm (20 lp/mm), the spatial length of each pixel must correspond to 25 μm at least. Although the resonant driving of the horizontal mirror leads to a sine-like deflection of the illumination beam, the digitization of the backscatter signal was performed linearly in time with the acquisition card. This leads to a nonlinear deformation of the x axis in the image. This effect is reduced by taking only 50% of the resonant scanning cycle. For an FOV of 21×21 mm and to resolve the maximum optical resolution two scanning variations were used. In one realization, the full half period (π) of the oscillating fast mirror is used for sampling. With this realization, the pixels that correspond to the nonlinear part of the sinusoidal mirror movement shows strong distortion. These distortions were faced with an alternative realization, which uses only the linear slope of the sinusoidal mirror movement using the pixels that correspond to a quarter period ($\pi/2$) of the fast mirror oscillation. Using these two acquisition variations, the minimum sampling rates can be extracted for square pixels (1:1 aspect ratio).

1. For π sampling, 840 samples are required per line (21 mm/25 μm), resulting in a minimum pixel sampling frequency of approximately 2 Msamples/s. The frame acquisition time is 840 times the line scanning duration, resulting in 0.349 s and a maximum frame rate of 2.86 frames/s.
2. For $\pi/2$ sampling with similar reasoning, 1680 samples are required per line, resulting in a minimum pixel sampling frequency of approximately 4 Msamples/s and a maximum frame rate of 1.43 frames/s.

The sampling consideration just referenced are theoretical calculations, and in practice the higher spatial frequencies usually have low power and aliasing is seldom observed.

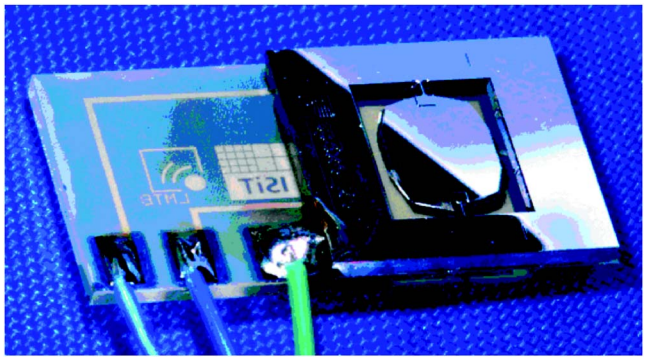

Fig. 3 Picture of a scanning micromirror. The mirror plate with its support, the substrate, and the control electrodes are shown.

To increase the image frame rate, mirrors with higher oscillating frequencies are required, which with the current manufacturing process results in smaller deflection angles. From the preceding calculations, the optical detector must have a bandwidth of at least 4 MHz, and the acquisition card must also have a bandwidth of 4 MHz and be able to support a minimum sampling rate of 4 Msamples/s.

The acquisition board selected has a bandwidth of 5 MHz and can sample all the color channels at 5 Msamples/s simultaneously. According to the preceding, in the current realization, the endoscope bandwidth is restricted from the signal levels that can be detected from the detectors selected, resulting in 5 MHz for the red channel and the C5460 APD and 100 kHz for color imaging using the C5460-1 photodetector.

2.2 *Laser Scanning Micromirrors*

The micromachined scanning mirrors used are similar to the scanner setups described elsewhere[8,9] and are electrostatically driven and controlled (Fig. 3). The scanners consist of an Aluminum coated Silicon mirror plate that is laterally suspended by two torsional Nickel springs. The mirror plate has a thickness of 20 microns. Nickel has the great advantage over Silicon that it is not brittle and so it does not break that easily. The torsional Nickel springs suspend the movable mirror in a surrounding silicon frame (Fig. 3). This wet-etched structure is mounted onto a Pyrex substrate with two integrated electrodes and connector terminals. The electrodes are oriented parallel to the mirror axis, so that each of them is below one half of the mirror. For operation, a positive voltage U_{drive} is applied to one electrode and an equal negative voltage to the other electrode, while the mirror is biased with the voltage U_{bias}.

The electrostatically controlled mirrors can be modeled with a capacitor with parallel plates, one of which is rotated. For a parallel-plate capacitor, the electrostatic force can be found by taking the derivative of its stored electrical energy[11,12]

$$F(x) = \frac{\mathrm{d}}{\mathrm{d}y}\frac{CV^2}{2} = \frac{V^2}{2}\frac{\mathrm{d}}{\mathrm{d}y}\left(\frac{\varepsilon A}{y}\right) = -\frac{V^2}{2}\frac{\varepsilon A}{(h-\varphi x)^2}, \tag{5}$$

where y is the distance between the two plates, h is the distance between the two plates when the mirror is in the rest position, φ is the angle of rotation, and x is the distance

from the rotation axis. From Eq. (5) it follows that the force, to a good approximation, is proportional to the square of the applied voltage V between the two plates.

Consecutively, the electrostatic force created between each electrode and the mirror causes two torques that are also proportional to the applied voltage $V|M_1| \propto (U_{\text{bias}} - U_{\text{drive}})^2$ and $|M_2| \propto (U_{\text{bias}} + U_{\text{drive}})^2$, respectively. The resulting total torque is not proportional to the square of the drive voltage and is approximated with the following equation.

$$M_{\text{total}} = M_2 - M_1 \propto (U_{\text{bias}} - U_{\text{drive}})^2 - (U_{\text{bias}} + U_{\text{drive}})^2 = 4U_{\text{bias}}U_{\text{drive}}. \quad (6)$$

Obviously, by applying an appropriate nonzero bias voltage, the relation between the applied voltage and the mirror deflection angle was linearized.[8] The voltage U_{drive} ranges from 100 to 400 V, depending on the bias voltage and the required FOV.

The fast scanner is generally driven on resonance. In this work, different scanners with frequencies between 500 Hz and 1.2 kHz were developed and tested. The higher is the resonant frequency, the lower is the mirror deflection achieved for a given driving voltage. As a result, there is a trade-off between the image acquisition speed and the FOV obtained. By contrast, the slow scanner has a resonant frequency around of 50 Hz and is operated quasi-statically. The realized mirrors had dimensions of 4×4.8 and 3×4 mm^2 for the slow and fast mirrors, respectively. The slow mirror should have larger dimensions due to the walking effect of the laser beam that is present in the serial mirror arrangement followed.

The arrangement of the micromirrors is crucial for maximizing the achievable FOV. Each mirror is capable of performing a rotation of up to ±2.5 deg around its axis, which translates to a beam deflection of ±5 deg for a beam incident perpendicularly on the mirror surface when it is in the rest position. This optimal condition cannot be ensured in a miniaturized endoscope head; however, in our case, the angle of incidence on the scanner was kept as perpendicular as possible by using a suitable prism for beam deflection.

2.3 *Data Acquisition, Processing, and Control Unit*

An important part of the entire device is the data acquisition, control, and processing (DACP) unit. This unit is responsible for the control of the scanning operation (by driving the scanning micromirrors with appropriate voltage waveforms), the image reconstruction of the scanned target from the detected optical signals; and the preprocessing, storage, and display operations in real time. Details about the DACP unit are presented elsewhere.[13,14]

The DACP unit simultaneously digitizes the three electrical signals (one for each color) that are generated at the outputs of the optical detection units and provides the two analog waveforms required for the position control of the scanning micromirrors used. After digitization, the reconstruction, preprocessing, and display operations are performed in real time with the multiprocessor PC system employed.

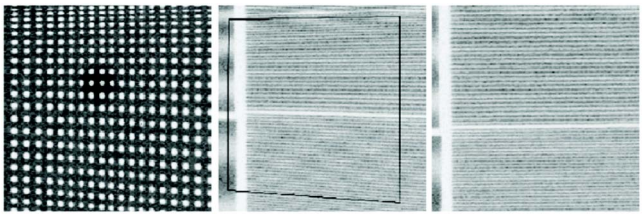

Fig. 4 Left, rectangular dot pattern imaged with the endoscope showing trapezoidal distortion. The diameter of each dot is 0.25 mm and the dot spacing is 0.5 mm. Center, distorted line pattern as recorded with the endoscope. Right, the same line pattern after removing the trapezoidal distortion mathematically.

The principal module of the data acquisition and control subsystem is a commercially available data acquisition card (the PCI-6110E from National Instruments Co.). Using this card, a simultaneous digitization of the three analog signals is performed with a maximum sampling frequency of 5 Msamples/s per channel along with the generation of the two control voltage waveforms.

A dual CPU Symmetric multiprocessor system was employed along with the appropriate multithreaded software that provides the parallel execution of time-consuming program modules into the available processors. The multithreaded approach followed here has proven invaluable as it ensured predictable responsiveness to hardware-generated control events and commands through the user interface together with increased performance.

3 Optical Behavior and Characterization of the Endoscope System

In this section, a short analysis of the optical distortions of the endoscope system is presented together with procedures for objective measurement and correction. The resolution of the endoscope system is objectively measured using its modulation transfer function and the effects that deteriorate its value are also discussed. Finally, first results of imaging of technical and biological objects with the realized endoscope prototype are presented.

3.1 *Analysis and Correction of Field Distortions*

The scanners of the device and their geometrical layout inside the scanning head induce a moderate distortion to the image, even after correcting it for the sinusoidal motion of the fast scanning mirror. This distortion is clearly demonstrated when the image of a regular, rectangular dot pattern is observed (Fig. 4, left).

To correct the distortion by means of image postprocessing, for each object point $P_o(x_o, y_o)$ the corresponding distorted image point $P_i(x_i, y_i)$ was determined using a suitable algorithm. Utilizing these data, two bicubic spline interpolating surfaces were calculated through the set of the coordinates x_i and y_i, respectively. Then, for a given image coordinate, the corresponding undistorted object coordinate can be computed and the undistorted image can be extracted by appropriately interpolating the recorded pixel array.

This technique was applied on a test line pattern (Fig. 4, center) and we found that it successfully removed the trapezoidal distortion (Fig. 4, right).

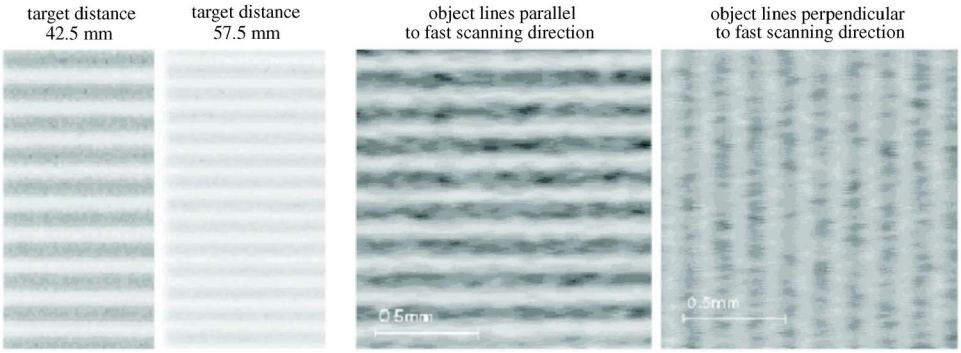

Fig. 5 Left, sinusoidal line pattern with a spatial frequency of 1.5 lines/mm at different object distances; right, another test pattern in horizontal and vertical orientation. The suboptimal synchronization between the horizontal fast forward and backward movement of the scanning beam deteriorates contrast.

3.2 *Modulation Transfer Function of the Microscanning Endoscope*

The modulation transfer function (MTF) of the endoscope was measured using a set of sinusoidal line patterns, of various spatial frequencies, for different target distances around the focal length (Fig. 5). The line pattern could be parallel or perpendicular to the fast scanning direction, enabling extraction of the horizontal and vertical MTFs, respectively.

The contrast is generally very low and lies under 0.5, even for low spatial frequencies. This low contrast is certainly due to a weak signal, resulting from insufficient collected light due to the small NA. At low spatial frequencies, the contrast should be close to 1 when an adequate signal is collected.

In both graphs shown in Fig. 6, it can also be seen that, at low spatial frequencies, the shorter the target distance the higher is the contrast [Fig. 6(a)]. For low spatial frequencies, the contrast is not significantly affected by defocusing and possibly is much more dependent on the amount of collected light, which is significantly higher at short target distances. For higher spatial frequencies, focusing becomes prevalent. For optimal focusing, the maximum detail resolution has been found to be 16 lp/mm.

As the image is obtained by horizontally scanning the target, the MTF is different for horizontal and vertical image structures. This difference is due to loss of the scanning synchronization. The image is formed line per line, one line acquired from left to right and the next one from right to left (bidirectional scanning). Although these two scans are regularly synchronized, they present in fact a small shift. This shift does not affect horizontal resolution, but affects the vertical resolution [Fig. 6(b)].

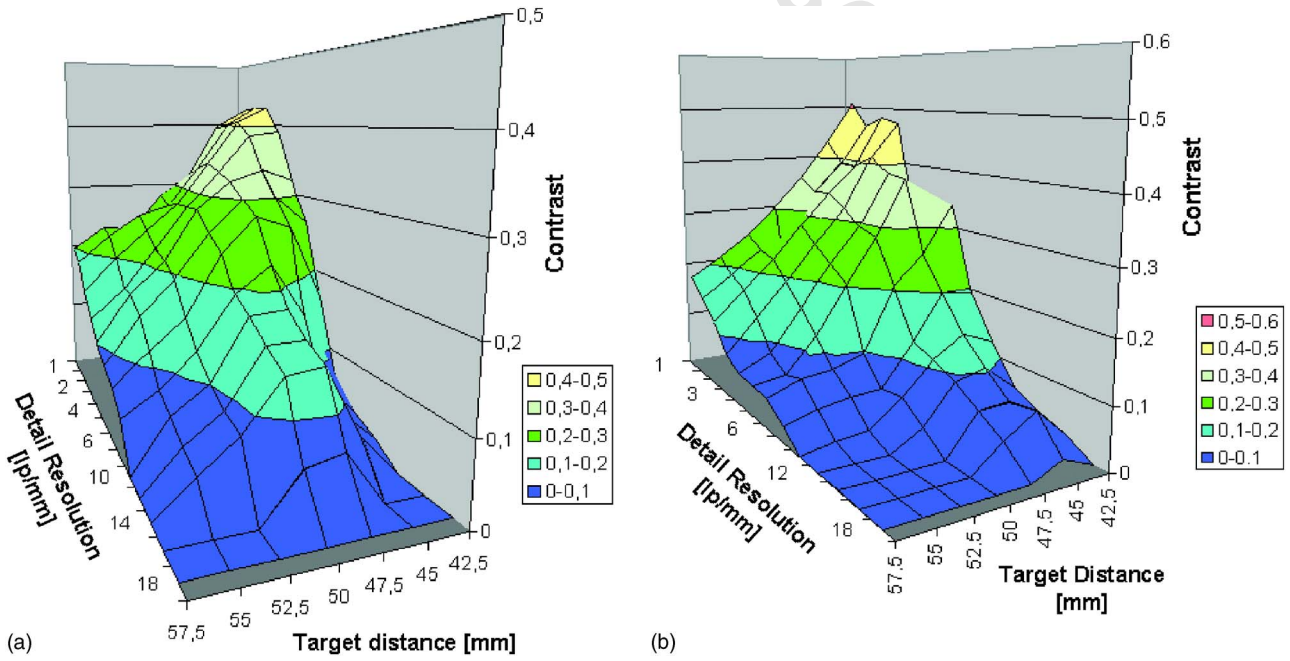

Fig. 6 (a) Horizontal and (b) vertical MTFs.

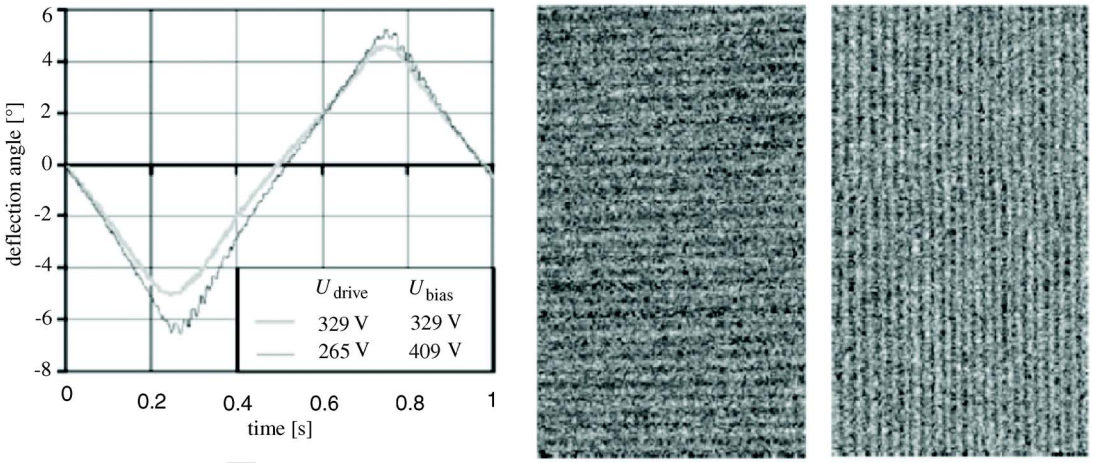

Fig. 7 Resolution along the slow scanning direction can be deteriorated by mirror oscillations. Left, rotation of the slow scanning mirror while being addressed by a triangular control voltage. The rapid change in direction excites the resonance of the mirror, which leads to an oscillation. Right, the exited oscillation for a saw tooth drive voltage causing the resolution in the slow scanning direction to be worse than in the fast scanning direction. The object is a Ronchi grating with 12.5 lines/mm.

3.3 *Resolution Deterioration Caused by Mirror Oscillations*

While the fast mirror is driven in resonance, performing a harmonic oscillation movement, the slow mirror is operated quasi-statically, to ensure a movement corresponding to the control-voltage pattern applied. Mathematically, the ideal signal form for this control voltage is a triangular waveform for bidirectional image acquisition and a saw tooth waveform for unidirectional image acquisition. In the present realization presented, care has been taken for avoiding the excitation of eigenoscillations of the slow mirror, which would reduce the vertical resolution (Fig. 7). As the control voltage for the slow mirror is a triangular waveform, these oscillations were nearly completely avoided with an adequate choice of the bias voltage and the appropriate selection of certain parameters of the control waveform that determine its shape in the fast transition regions.[13]

3.4 *Imaging of Technical and Biological Objects*

Since the contrast achieved with the endoscope is limited, due to the low NA, the imaging of samples with small color or brightness variations tends to be difficult. Best results are obtained for technical objects. In the pictures shown in Fig. 8 the optical powers emerging from the illumination fiber were found to be 8, 5, and 8 mW, for the red, green, and blue channels, respectively. The maximum voltage levels measured at the outputs of the corresponding APD amplifiers were about 2.7 V and 400 and 150 mV, respectively. As expected (Table 1), the efficiency of the blue channel is the worst one.

Imaging of biological objects has been also performed with the developed prototype system. Figure 9 shows an image of heart tissue. The image was acquired using the red channel of the MEDEA (microscanning endoscope with diagnostic and enhanced resolution attributes) setup. The FOV is about 11×11 mm and the dynamic range is roughly 5 bits. The image was acquired in the bidirectional mode using a 100-kHz Hamamatsu APD and a sampling frequency of about 1.2 MHz. The number of pixels is 1024×1024, whereas about 400 pixels are optically resolved. The main structures in the front of the image are sharply defined and imaged with high contrast. These structures are in a size range of some 100 μm up to 1 mm. Therefore, we can conclude that the optical resolution is much better close to about 20 lp/mm.

4 Discussion and Conclusions

A fully operational prototype of a color laser scanning endoscope was designed, assembled, and tested. This specific realization used a semiconfocal optical design that in combination with the laser-scanning technology provides high resolution due to the fact that the scanning spot dimension determines the resolution and not the size of the area from which the backscattered signal is detected. As a result, this

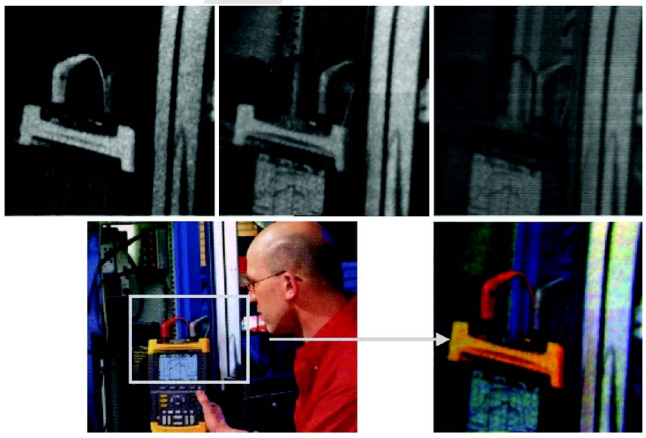

Fig. 8 Bottom left, Color photography with a marked region of interest of 18×15 mm; bottom right, region of interest as composed from the three channels of the color laser scanning endoscope after gray-value equalization; top from left to right, sequentially recorded channels for the red, green, and blue lasers.

Fig. 9 Part of heart tissue (*in vitro*) with an FOV of 11×11 mm for the red channel. The number of optically resolved points is about 400/line ($\pi/2$ sampling). The dynamic range is approximately 5 bits.

device offers enhanced resolution together with large FOV and depth of focus, while the optical design followed provides rejection of tissue surface reflections.

The use of lasers for illumination makes the device principally multifunctional, as different diagnostic image formation processes can be employed in that case. The scanning approach is mainly responsible for the high resolution, since the single-point illumination makes the device at least semiconfocal. Therefore, the contrast generation at the sample is far superior compared to modern endoscopy techniques, which use wide-field illumination.

In the presented system, because of the low NA, only a small portion of the backscattered light can be collected, which clearly reduces contrast and SNR significantly. Hence, it must be doubted whether early lesions could be detectable when the operation is based on the backscattering signal alone. In addition, the FOV is limited by the achievable deflections of the scanning mirrors. Therefore, as yet, in its present state, the device cannot substitute for modern video endoscopes. Nevertheless, with this prototype a means for endoscopic laser-scanning imaging is available that could be used for many diagnostic laser applications discussed today. Photodynamic, fluorescence lifetime, laser-induced fluorescence or autofluorescence imaging could be performed. Note also that multiphoton imaging requires sufficient focal intensities, which might not be reached for the currently large working distances of the device.

For real endoscopic use, the system should be upgraded by installing a focusing mechanism, which could be realized by means of displacement, moving axially the ends of the optical fibers inside the endoscope head.

A miniaturization to a diameter of 8 mm seems possible by manufacturing smaller micro-optics, especially the beamsplitters. Under consideration of the given specifications for FOV and NA, a further reduction of the outer diameter of the optical head (which is important for stereoscopic endoscopes) requires other concepts for the tilting mirror, i.e., without outer frames or a gimball topology. A gimballed scanning mirror[13] aside from size reduction of the device will minimize the losses due to scattering, the mirror surface absorption, and wavefront deformation.

Acknowledgments

This work has been supported by the Commission of the European Communities in the framework of the BIOMED2 European Project with the title "MEDEA Micro-scanning Endoscope with Diagnostic and Enhanced Resolution Attributes" under Contract No. BMH4-CT97-2399. The authors also appreciate the efforts of G. Anagnostopoulos, P. Dario, C. Stefanini, G. Delacretaz, U. Hofmann, K. Dorschel, R. Schutz, J. Knittel, and W. Junger for their contributions to the project.

References

1. T. Lange, "State of the art of video techniques for endoscopic surgery," *Endosc Surg. Allied Technol.* **1**, 29–35 (1993).
2. A. Cuschieri, G. Buess, and J. Perissat, *Operative Manual of Endoscopic Surgery*, Springer, Heidelberg (1992).
3. N. Ramanujam, J. X. Chen, K. Gossage, R. Richards-Kortum, and C. Britton, "Fast and noninvasive fluorescence imaging of biological tissues *in vivo* using a flying-spot scanner," *IEEE Trans. Biomed. Eng.* **48**(9), (2001).
4. D. Shotton, *Electronic Light Microscopy, Techniques in Modern Biomedical Microscopy*, Chap. 12, Willey-Liss (1993).
5. D. L. Dickensheets and G. S. Kino, "Silicon-micromachined scanning confocal optical microscope," *J. Microelectromech. Syst.* **7**, 38–47 (1998).
6. W. Piyawattanametha, H. Toshiyoshi, J. LaCosse, and M. C. Wu, "Surface-micromachined confocal scanning optical microscope," in *Proc. Lasers and Electro-Optics, 2000 (CLEO 2000)* (2000).
7. G. J. Tearney, M. E. Brezinski, B. E. Bouma *et al.*, "In vivo endoscopic optical biopsy with optical coherence tomography," *Science* **276**(5321), 2037–2039 (1997).
8. U. Hofmann, S. Muhlmann, M. Witt, K. Dorschel, R. Schutz, and B. Wagner, "Electrostatically driven micromirrors for a miniaturized confocal laser scanning microscope," in *Miniaturized Systems with Micro-Optics and MEMS*, *Proc. SPIE* **960**, 29–38 (1999).
9. M. George, H. Albrecht, M. Schurr, P. Papageorgas, U. Hofmann, D. Maroulis, C. Depeursinge, D. Iakkovidis, N. Theofanous, and A. Menciassi, "A laser-scanning endoscope based on monosilicon micromachined mirrors with enhanced attributes," in *Novel Optical Instrumentation for Biomedical Applications*, *Proc. SPIE* **5143**, 145–156 (2003).
10. T. J. Farrell, M. S. Patterson, and B. Wilson, "A diffusion theory model of spatially resolved, steady-state diffuse reflectance for the non-invasive determination of tissue optical properties in vivo," *Med. Phys.* **19**(4), 879–888 (1992).
11. *The Feynman Lectures on Physics*, Vol. 2, Chap. 8, pp. 779–782, Narosa Publishing, (1964).
12. M. N. Horenstein, T. G. Bifano, R. Mali Krishnamoorthy, and N. Vandelli, "Electrostatic effects in micromachined actuators for adaptive optics," *J. Electrost.* **42**, 69–81 (1997).
13. P. Papageorgas, D. Maroulis, H. Albrecht, B. Wagner, G. Anagnostopoulos, M. Schurr, N. Theofanous, P. Dario, and C. Depeursinge, "The data-acquisition, processing and control system of a micromirror-based laser-scanning endoscope," in *Proc. IEEE Int. Conf. on Circuits and Systems*, pp. 1203–1206 (2002).
14. G. Anagnostopoulos, B. Wagner, P. Papageorgas, U. Hofmann, D. Maroulis, and N. Theofanous, "The electronics of a control system for micromirrors in a laser-scanning device," in *Proc. IEEE Int. Conf. on Circuits and Systems*, pp. 1207–1210 (2002).

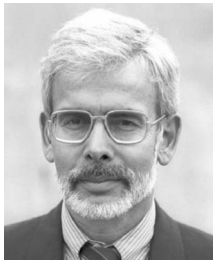

Hansjörg Albrecht received a BSc in physics from Stuttgart and Hamburg Universities in 1969 and a PhD in 1976. From 1969 until 1971 he worked as a development engineer in AEG-Telefunken, Berlin, and from 1971 until 1978 he worked as a scientist in the Central Institute for Biomedical Engineering, Erlangen-Nuremberg University. From 1978 until 1983 he worked as a scientist with DFVLR and from 1984 until 1989 he was head of product management monitoring with Dräger AG, Lübeck. From 1989 until 1990 he was a scientific adviser at Laser-Medizin-Zentrum (LMZ), Berlin, and head of the Physicochemical Technologies Department. In 1990 he became the managing director of LMZ Berlin, which was reorganized in 1995 into LMTB, and since 2003 he has been the general manager of LMTB.

Panagiotis G. Papageorgas received a BSc in physics and a PhD in applied physics from the University of Athens in 1984 and 1995, respectively. From 1985 to 1991, he worked as a teaching assistant with a doctoral fellowship in the Laboratories of Electronics and Meteorology of the Department of Applied Physics at the University of Athens. His dissertation research was on the development of sound detection and ranging (SODARs). Since 1994 he has been with the Department of Informatics and Telecommunications, Division of Communications and Signal Processing of the same university, as a researcher in European projects in the development of electronic instrumentation for air pollution, biomedical applications, and electronic imaging. He is currently an associate professor in the Department of Electronics of the Technological Educational Institute of Piraeus.

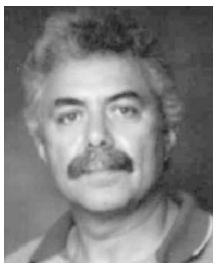

Dimitris Maroulis received a BSc in physics, a MSc in radioelectricity, a MSc in cybernetics, and a PhD in informatics, all from the University of Athens, Greece, in 1973, 1977, 1980, and 1990, respectively. In 1991 he was elected as a lecturer and in 1994 he was elected as an assistant professor, in the Department of Informatics of the same university. He is currently working in the above department in teaching and research activities, including projects with the European Community. His main areas of activity include data acquisition systems, real-time systems, image analysis, and biomedical systems.

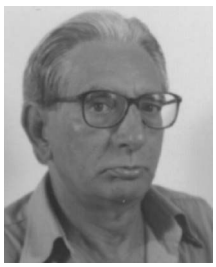

Nikiforos G. Theofanous received a BSc in physics, a MS in radioelectricity, a PhD in physics, and a MSc in electronic automation, all from the University of Athens, in 1964, 1971, 1973, and 1975, respectively. In 1969 he was appointed as an assistant and in 1973 he was elected as chief assistant in the Electronics Laboratory, University of Athens, for the period up to 1981. In 1982, he was elected as a lecturer and in 1984 as an assistant professor, in the Department of Physics, University of Athens. In 1990, he was transferred to the Department of Informatics of the same university, where, in 1991, he was elected associate professor and in 1995 full professor in electronics and optoelectronics. He is currently working in the above department in teaching and research activities, including projects with the European Community. He is president of the Greek Laser & Electrooptics Scientific Society and his main areas of activity include electro-optics, fiber optics, and optoelectronics with applications in optical communications and in optoelectronic biomedical systems.

Stavros A. Karkanis obtained his BSc in mathematics from the University of Athens, Greece, in April 1986 and his PhD in 1995 from the Department of Informatics and Telecommunications of the same university. For the last 17 years he has been working in the field of image processing and especially in the area of texture recognition from various academic and industry positions. Today he is an associate professor in the Department of Informatics at the Technological Educational Institute of Lamia. His main interests include texture recognition, wavelet transforms for texture, pattern recognition for image processing applications, and statistical learning methodologies for classification.

Bernd Wagner received his physics diploma and PhD from University of Mainz in 1982 and 1986, respectively. He joined Fraunhofer-Institute for Silicon Technology (ISIT) working on design, technology, and application development of microsystems. Presently, Dr. Wagner is head of the Microsystems/MEMS Department at Fraunhofer ISIT in Itzehoe. His current research activities are focused on silicon-based sensors and actuators, optical microsystems, and RF-MEMS. He has authored or co-authored more than 80 scientific publications.

Marc Schurr has been working in medical research since 1990, after graduation from medical school. His scientific results have led to a significant number of publications and conference presentations. From 1996 to 2002 he was director of Steinbeis Transfer Centre Healthcare Technologies and was also in charge of the research program into advanced technology at the section for minimally invasive surgery at Eberhard-Karls University, Tuebingen, Germany. In this function he has initiated and directed a number of international R&D projects. He is director of the Institute of Healthcare Industries (IHCI) at Steinbeis University Berlin, where he is professor of management and technology in healthcare. He is member of the boards of several companies and associations and entertains close contacts to leading European and American corporations and scientific institutions. From 2000 to 2001 he was president of the Society for Medical Innovation and Technology.

Christian Depeursinge is the leader of the Microvision and MicroDiagnostics (MVD) group in the Institute of Applied Optics (IOA) at EPFL (Ecole Polytechnique Fédéralede Lausanne), Switzerland. His current research interests include coherence and incoherent imaging applied to nanodiagnostics and nanoassembly in biology. In particular digital holographic microscopy (DHM) aims at nanotechnology developments and research in the life sciences. These techniques are developed for living tissues analysis and spectroscopy. "*In vivo* biopsy" techniques are also part of the research topics of the MVD group.

Arianna Menciassi received her Laurea degree in physics (with honors) from the University of Pisa in 1995. In the same year she joined the CRIM Lab of the Scuola Superiore Sant'Anna (SSSA) in Pisa as a PhD student in bioengineering with a research program on the micromanipulation of mechanical and biological micro-objects. In February 1999, she received her PhD degree. The main results of the activity on micromanipulation were presented at the IEEE International Conference on Robotics & Automation (May 2001, Seoul) in a paper titled "Force feedback-based microinstrument for measuring tissue properties and pulse in micro-

surgery," which won the "ICRA2001 Best Manipulation Paper Award." In 2000, she was offered a temporary position of assistant professor in bioengineering at SSSA and she still has this position. Her main research interests are in the fields of biomedical microrobotics, microfabrication technologies, micromechatronics, and microsystem technologies. She is working on several European projects and international projects for the development of minimally invasive instrumentation for medical applications and for the exploitation of micro- and nano-technologies in the medical field. Dr. Menciassi is an author of more than 20 ISI journal papers and about 50 conference papers; she is a member of the IEEE Robotics and Automation Society and of the Engineering in Biology and Medicine Society.